assembly ($y \approx 17$ mm). Figure 2 indicates that significant average unmixedness exists at the exit plane of the assembly for the reference angle $\theta = 0$ deg. The images also demonstrate that small positive changes in θ tend to further degrade the mixing efficiency of this assembly. However, a small negative rotation to an orientation of $\theta = -20$ deg results in a much more uniform fuel distribution across the fuel/air jet.

Similar results are shown for the second fuel-tube configuration in Fig. 3. As compared to the first fuel-tube configuration, this module displays improved mixing efficiency at its base reference angle. In response to changes in θ, positive rotation of the fuel tube once again decreases the mixedness of the fuel-airflow. However, for this case the base orientation, rather than a slightly negative fuel-tube angle, seems to provide optimal mixing. The implication is that fuel-jet mixing occurs primarily via crossflow of preswirler air over the fuel tube. As shown by Fig. 3, the second configuration has the additional benefit of being less sensitive to small changes in fuel-tube angle.

Finally, we determined how rapidly mixing occurred within the fuel-air stream as a function of downstream distance. Because these fuel/air streams enter into a larger swirler assembly prior to combustion, unmixedness at the exit of the swirler-vane/fuel-tube assembly is only a problem if it persists into the reaction zone. Figure 4 shows fuel-concentration distribution as a function of distance from the fuel tube, along the fuel-air jet, for the second fuel-tube configuration ($\theta = 0$ deg). Although a fair amount of unmixedness occurs at the exit plane (17 mm), nearly complete fuel-air mixing occurs at $\sim$23 mm from the fuel-tube centerline and well before the end of the swirler-vane module. In fact, at this location the average fuel mole fraction is 0.083 as compared to the fully mixed mole fraction of 0.05.

Conclusion

In conclusion, simple qualitative measurements of the type presented in this study can be crucial to optimization of fuel-air mixedness and thus minimization of NO_x emissions from lean premixed combustors. Additional parameters such as fuel type, fuel/air momentum ratio, or air preheat temperature can be effectively studied on both a spatial- and time-averaged basis via acetone PLIF measurements of surrogate fuel.

Acknowledgments

This work was supported by a contract from Rolls-Royce/Allison (Indianapolis, IN), with Mohan Razdan as research monitor. The authors would like to acknowledge Steve Frey at Rolls-Royce/Allison for his design and development of the swirler-vane/fuel-tube assemblies used in this investigation.

References

[1]Correa, S. M., "Power Generation and Aeropropulsion Gas Turbines: from Combustion Science to Combustion Technology," *Proceedings of the Twenty-Seventh International Symposium on Combustion*, Combustion Inst., Pittsburgh, PA, 1998, pp. 1793–1807.

[2]Fric, T. F., "Effects of Fuel-Air Unmixedness on NO_x Emissions," *Journal of Propulsion and Power*, Vol. 9, No. 5, 1993, pp. 708–713.

[3]Puri, R., Stansel, D. M., Smith, D. A., and Razdan, M. K., "Dry Ultralow NO_x "Green Thumb" Combustor for Allison's 501-K Series Industrial Engines," *Journal of Engineering for Gas Turbines and Power*, Vol. 119, No. 1, 1997, pp. 93–101.

[4]Lozano, A., Yip, B., and Hanson, R. K., "Acetone: a Tracer for Concentration Measurements in Gaseous Flows by Planar Laser-Induced Fluorescence," *Experiments in Fluids*, Vol. 13, No. 6, 1992, pp. 369–376.

[5]Lozano, A., Smith, S. H., Mungal, M. G., and Hanson, R. K., "Concentration Measurements in a Transverse Jet by Planar Laser-Induced Fluorescence of Acetone," *AIAA Journal*, Vol. 32, No. 1, 1993, pp. 218–221.

[6]Frazier, T. R., Foglesong, R. E., Coverdill, R. E., Peters, J. E., and Lucht, R. P., "An Experimental Investigation of Fuel/Air Mixing in an Optically Accessible Axial Premixer," AIAA Paper 98-3543, July 1998.

Radiation and NO_x Pathways in Nonpremixed Turbulent Flames

D. Lentini*
University of Rome "La Sapienza," I–00184 Rome, Italy
and
I. K. Puri†
University of Illinois at Chicago, Chicago, Illinois 60607-7022

Introduction

CURRENT demanding standards require accurate predictions of NO_x outflow from flames and combustors. Turbulent flows hamper a detailed accounting of NO_x formation; the standard approach considers only the thermal pathway in adiabatic conditions. However, NO_x formation involves different pathways[1]: thermal, nitrous oxide, prompt, nitric dioxide, and fuel.

This investigation introduces a treatment for heat losses by radiation in optically thin nonsooting flames and explores the reaction regimes of the various NO_x pathways. The model is based on the stretched laminar flamelet (SLF) approach, which considers a turbulent flame to consist of thin laminar flamelets. Chemical processes characterized by a timescale shorter than the Kolmogorov time t_K contribute to the definition of their structure, whereas those involving a timescale larger than t_K occur in the distributed reaction regime; a finer division discriminates between the regions $t_K < t_c < t_I$ and $t_c > t_I$, where t_I is the integral scale. Provided that the processes are energetically insignificant (as in the case of NO_x) and uncoupled from faster paths a treatment can be devised for the latter regime as well.

Central to the SLF approach is the identification of the characteristic chemical time of the different NO_x pathways. This paper defines the elements required to investigate the reaction regime of the thermal and N_2O pathways.

Treatment of Heat Loss Effects via the SLF Approach

An extension of the SLF formalism to nonadiabatic combustion, as suggested in Ref. 2, has recently been developed.[3] It is based on the introduction of an enthalpy defect given in the following equation, in addition to the conserved scalar (or mixture fraction, defined in terms of enthalpy) Z and the scalar dissipation rate χ_c (conditioned at the flame front):

$$\zeta = h - [h_o + Z(h_f - h_o)] \tag{1}$$

that is, the gap between the actual enthalpy and that of an adiabatic flame (h_o, h_f refer to oxidizer and fuel). State quantities in laminar flames can then be expressed as

$$\phi = \phi(Z; \chi_c; \zeta) \tag{2}$$

so that average values can be recovered by convolution with an appropriately defined joint probability density function (PDF) of Z, χ_c, and ζ. The approach requires an additional equation for $\tilde{h}$, to recover $\tilde{\zeta}$ after averaging the linear relationship (1). The SLF model for turbulent flames requires as an input a library of laminar flames, with properties expressed in form (2). Profiles must be organized in shelves, where each shelf contains entries for numerous χ_c values from equilibrium to extinction plus the inert (or pure-mixing) state, and each shelf refers to a different value of ζ.

Received 20 December 1997; revision received 29 October 1999; accepted for publication 9 December 1999.

*Associate Professor, Department of Mechanics and Aeronautics, Via Eudossiana 18.

†Professor, Mail Code 251, Department of Mechanical Engineering, 842 W. Taylor Street.

In the test case discussed next, heat loss is due to gas-phase radiation alone and the optically thin limit can be reasonably assumed due to the small flame size. The heat loss term in the enthalpy equation is

$$\operatorname{div} \boldsymbol{q}_r = 4\sigma p[T(Z, \chi_c, \zeta)]^4 \sum_i k_i[T(Z, \chi_c, \zeta)]X_i(Z, \chi_c, \zeta) \quad (3)$$

where $\boldsymbol{q}_r$ is the radiative heat flux, σ is the Stefan–Boltzmann constant, p is the pressure, and k_i are the absorption coefficients (functions of temperature only) in terms of partial pressure of the relevant species, whose molar fraction is X_i. Equation (3) has form (2) and can be averaged accordingly. The sum in Eq. (3) is extended to the radiating species H_2O, CO_2, and CO.

Impact of Radiation from a Turbulent Syngas/Air Flame

The model is applied to a nonpremixed turbulent syngas/air flame, investigated both experimentally[4] and numerically (assuming adiabatic flow), for example, see Refs. 4 and 5. The flamelet library is computed in the Z space,[6] neglecting differential diffusion. The scalar dissipation rate $\chi_{\max}$ is evaluated at the maximum temperature. Four shelves at $\zeta = 0, -20, -40, -60$ kJ/kg are considered.

For the turbulent flame, $\tilde{\zeta}$ is recovered with $\tilde{h}$ computed via its modeled conservation equation; the minimum in the entire flowfield is $\tilde{\zeta} = -48$ kJ/kg. The mean concentration of thermal NO is also computed via a modeled conservation equation, where the mean production term is expressed by convolution with the PDF because of its very slow kinetics. The simulation is carried out on a 100×2300 node grid, to ensure full grid-independent solution (if the number of both radial and axial nodes is halved, the predicted flame length is affected by just 0.6%).

The reduction in predicted NO_x outflow due to radiation is limited to 12% with respect to an adiabatic flame, that is, from 3.27×10^{-8} to 2.89×10^{-8} kg/s, to be compared to the measured 3.4×10^{-8} kg/s. This is an extremely good agreement for NO_x emissions, for example, Ref. 4 for the same case predicts 2.6×10^{-8} kg/s. Although accounting for radiation may seem to deteriorate the agreement, the computed outflow refers to thermal NO only, and neglected pathways are expected to increase the stated values.

Figure 1 compares the predicted mean mole fraction of NO (on dry basis) to measurements at station $x/D = 100$. The predicted flame length is about 42 fuel nozzle diameters; the station is then well into the postflame zone. The peak value is no longer overpredicted if radiation is included; however, far away from the axis NO levels are still too low, so that the total outflow is underpredicted.

Definition of Characteristic Chemical Times

Each NO_x pathway is characterized by its own chemical time $t_{c,k}$. For syngas, only the thermal and N_2O pathways are significant. The rate of the former ($k = 1$) is controlled by the step

$$N_2 + O \rightleftharpoons NO + N \quad \{1\}$$

followed by

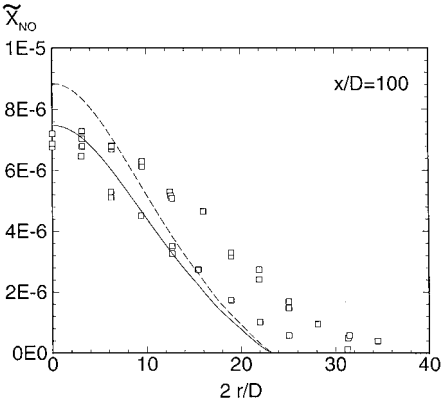

Fig. 1 Radial profiles of mean NO molar fraction (on dry basis) at x/D = 100: ——, and – – –, predictions with and without radiation, △, and □, experimental NO and total NO_x.

$$N + O_2 \rightleftharpoons NO + O \quad \{2\}$$

and

$$N + OH \rightleftharpoons NO + H \quad \{3\}$$

A typical time (concentration over production rate) for step {1} is

$$t_1 = Y_{NO}\left[W_{NO}B_1T^{\alpha_1}\exp(-T_{a,1}/T)\rho(Y_O/W_O)\left(Y_{N_2}/W_{N_2}\right)\right]^{-1} \quad (4)$$

Identification of the characteristic chemical time is deferred to later in this section. For the N_2O pathway ($k = 2$) the steps considered are

$$N_2 + O + M \rightleftharpoons N_2O + M \quad \{4\}$$

$$N_2O + H \rightleftharpoons NO + NH \quad \{5\}$$

$$N_2O + O \rightleftharpoons NO + NO \quad \{6\}$$

The chemical time for step {4} is evaluated by recasting Eq. (4) for a three-body reaction:

$$t_4 = Y_{N_2O}\left[W_{N_2O}B_4T^{\alpha_4}\exp(-T_{a,4}/T)(\rho^2/W)\right.$$
$$\left.\times (Y_O/W_O)\left(Y_{N_2}/W_{N_2}\right)\right]^{-1} \quad (5)$$

Chemical times for reactions {5} and {6} are evaluated as (discussed further subsequently)

$$t_5 = Y_{NO}\left[W_{NO}B_5T^{\alpha_5}\exp(-T_{a,5}/T)\rho\left(Y_{N_2O}/W_{N_2O}\right)(Y_H/W_H)\right]^{-1} \quad (6)$$

$$t_6 = Y_{NO}\left[2W_{NO}B_6T^{\alpha_6}\exp(-T_{a,6}/T)\rho\left(Y_{N_2O}/W_{N_2O}\right)(Y_O/W_O)\right]^{-1} \quad (7)$$

Equations (4–7) are in form (2); however, we neglect the effect of ζ, given its small influence in this case. Conditions maximizing Y_{NO} generally occur at very low χ_c, whereas maximum production occurs at moderate to high χ_c. We will explore a two-dimensional neighborhood of the couple (Z, χ_c) that gives maximum concentrations, for example, down to a concentration $1/e$ of this maximum, thus defining a range of chemical times.

Two limiting situations may arise: 1) short times (with respect to a representative t_K) and 2) long times. In the former case, the contribution of the kth pathway can be expressed in form (2). To make sure that this condition is not violated, $t_{c,k}$ is chosen as the upper bound of the range. In the latter case, the contribution can be computed by introducing a conservation equation, provided $t_{c,k} > t_I$, and we define $t_{c,k}$ as the lower bound of the range. When the $t_{c,k}$ are of the same order as t_K, the regime cannot be anticipated a priori.

Equations (6) and (7) are not uniformely valid because Y_{NO} refers to pollutant generated by all pathways. However, near the maximum of N_2O concentration virtually all of the NO is formed through this channel so that Eqs. (6) and (7) are locally correct.

We now apply these concepts to the syngas/air flame. The chemical time for the thermal pathway is quite long; then we identify $t_{c,1}$ as the lower bound, giving $t_{c,1} = 52$ ms, in close agreement with accepted values. For the N_2O pathway, Fig. 2 presents the characteristic global time, sum of Eq. (5), and the minimum (this pathway being relatively slow as well) between Eqs. (6) and (7). The dashed curves bound the region where N_2O concentration is in a range $1/e$, or $1/e^2$, of the maximum. The result is $t_{c,2} = 0.40$ ms, of which 0.12 ms are taken for N_2O formation and the rest for conversion to NO. Considering a range $1/e^2$ does not substantially alter this result.

A finer flamelet calculation, with detailed molecular transport, is conducted by a counterflow flame code[7] to assess the relative weight of the two pathways at different stretch levels. Results in Fig. 3 refer to a lower strain rate of 500 s^{-1} (peak temperature 1796 K) and a higher one of 2000 s^{-1} (1536 K). Figure 3 presents the pathways associated with nitrogen chemistry, with the domain-integrated rates of species consumption in units of mol $m^{-2} \cdot s^{-1}$. The N_2O pathway

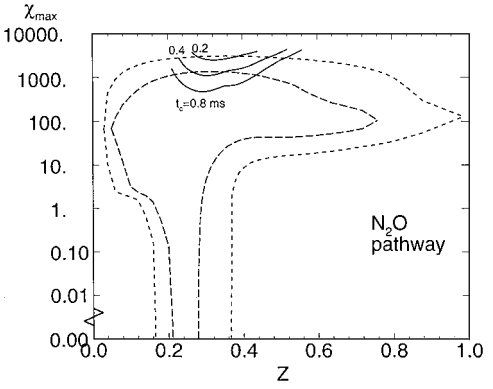

Fig. 2 Chemical times of N_2O pathway: – – –, and ----, isolines of concentration $1/e$ and $1/e^2$ of the peak, ——, isolines of chemical time.

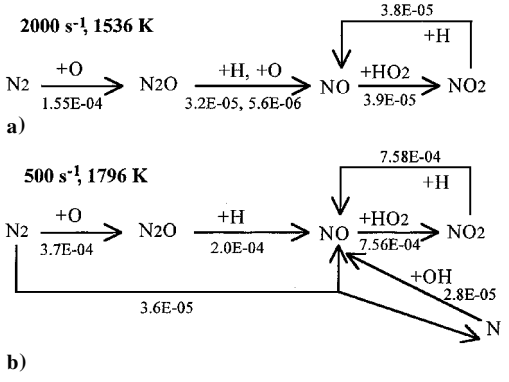

Fig. 3 Reaction pathway diagrams at a) a = 2000 s^{-1} and b) a = 500 s^{-1}.

is a major producer of NO at both rates, although at the lower stretch the thermal path is also active. At 2000 s^{-1}, although the rate of N_2 conversion to N_2O is 1.55×10^{-4} mol $m^{-2} \cdot s^{-1}$, through step {4}, the dominant path for N_2O conversion to NO (step {5}) has a far lower rate, that is, 3.2×10^{-5} mol $m^{-2} \cdot s^{-1}$. At 500 s^{-1}, although the rate of step {4} more than doubles, the conversion through step {5} is also significantly higher at 2×10^{-4} mol $m^{-2} \cdot s^{-1}$; the thermal pathway also produces NO. At both strain rates, virtually all the NO recycles itself rapidly through NO_2, resulting in a negligible net NO_2 formation, so that it is in steady state. N_2O is not in true steady state at either strain rate. This is induced by observing its net formation rate, which is 1.2×10^{-4} mol $m^{-2} \cdot s^{-1}$ (broadly comparable to its production rate) at 2000 s^{-1} and 1×10^{-4} mol $m^{-2} \cdot s^{-1}$ at 500 s^{-1} (only about 27% of its production rate).

Turbulent Reaction Regimes

The modeling of the different pathways depends on a comparison of their $t_{c,k}$ with the turbulent timescales. We consider the ratios $t_{c,k}/t_K$ and $t_{c,k}/t_I$ at the mean stoichiometric flame front. The thermal pathway is found to operate well into the $t_{c,1} \gg t_I$ regime, providing full justification for the standard approach. The N_2O pathway, however, is observed to operate in the condition $t_{c,2} > t_I$ only up to $x/D \simeq 12$ and in the regime $t_K < t_{c,2} < t_I$ thereafter. Both N_2O formation and its subsequent conversion to NO are found to occur individually in the latter regime. NO_x formation also occurs in the postflame zone.

Conclusions

An extension of the stretched laminar flamelet approach is used to account for radiation in nonpremixed turbulent flames. In the limited-size syngas/air flame under study, the predicted effect of radiation is to lower NO_x outflow by about 12%.

A criterion to identify characteristic reaction times for NO_x formation pathways is put forth and applied to the thermal and N_2O pathways involved in the test case. The resulting times are in agreement with available estimates.

The thermal pathway is found to operate in the regime $t_{c,k} > t_I$, whereas the N_2O pathway is found to operate across the regimes $t_{c,k} > t_I$ and $t_K < t_{c,k} < t_I$. The results are relevant for the development of predictive tools that allows for consideration of the N_2O pathway, in addition to the thermal channel.

References

[1]Miller, J. A., and Bowman, C. T., "Mechanism and Modeling of Nitrogen Chemistry in Combustion," *Progress in Energy and Combustion Science*, Vol. 15, 1989, pp. 287–338.

[2]Bray, K. N. C., and Peters, N., "Laminar Flamelets in Turbulent Flames," *Turbulent Reacting Flows*, edited by P. A. Libby and F. A. Williams, Academic Press, London, 1994, pp. 78–84.

[3]Marracino, B., and Lentini, D., "Radiation Modelling in Non-luminous Nonpremixed Turbulent Flames," *Combustion Science and Technology*, Vol. 128, 1997, pp. 23–48.

[4]Drake, M. C., Correa, S. M., Pitz, R. W., Shyy, W., and Fenimore, C. P., "Superequilibrium and Thermal Nitric Oxide Formation in Turbulent Diffusion Flames," *Combustion and Flame*, Vol. 69, 1987, pp. 347–365.

[5]Lentini, D., "Assessment of the Stretched Laminar Flamelet Approach for Nonpremixed Turbulent Combustion," *Combustion Science and Technology*, Vol. 100, 1994, pp. 95–122.

[6]Lentini, D., "Validation of a Formulation in Conserved Scalar Space for Stretched Laminar Flamelet Profiles," AIAA Paper 93-2200, July 1993.

[7]Rogg, B., "RUN-1DL: The Universal Laminar Flame and Flamelet Code," TR CUED/A–THERMO/TR39, Dept. of Engineering, Cambridge Univ., Cambridge, England, U.K., 1991.